Materials Research Express

PAPER • OPEN ACCESS

Fabrication and characteristics of $Zn_{1-x}Sn_xO$ nanorod/ITO composite photocatalytic films

To cite this article: Nguyen Dung T. *et al* 2020 *Mater. Res. Express* **7** 045504

Materials Research Express

PAPER

Fabrication and characteristics of $Zn_{1-x}Sn_xO$ nanorod/ITO composite photocatalytic films

Nguyen Dung T.[1], **Chien Dang Tran**[2], **Thien Trinh Duc**[3], **Anh Tuan Duong**[4], **Thang Pham Duc**[1], **Dinh Nguyen Nang**[1] **and Dinh Lam Nguyen**[1]

[1] Faculty of Engineering Physics and Nanotechnology, VNU University of Engineering and Technology, 144 Xuan Thuy Road, Cau Giay District, Hanoi, Vietnam
[2] Hanoi University of Natural Resources and Environment, 41A Phu Dien Road, North Tu Liem District, Hanoi, Vietnam
[3] Faculty of Physics, Hanoi National University of Education, 136 Xuan Thuy Road, Cau Giay District, Hanoi, Vietnam
[4] Phenikaa Institute for Advanced Study and Faculty of Materials Science and Engineering, Phenikaa University, Yen Nghia, Ha-Dong District, Hanoi 10000, Vietnam

E-mail: lamnd2005@gmail.com

Keywords: $Zn_{1-x}Sn_xO$ NRs/ITO, composite photocatalytic films, hydrothermal synthesis, photocatalyst, effective surface area, Sn dopant

OPEN ACCESS

RECEIVED
21 January 2020

REVISED
7 April 2020

ACCEPTED FOR PUBLICATION
17 April 2020

PUBLISHED
27 April 2020

Abstract

$Zn_{1-x}Sn_xO$ NRs/ITO composite photocatalytic films were fabricated by the hydrothermal method. A concentration of Sn dopant in $Zn_{1-x}Sn_xO$ nanorods (NRs) was varied from 0% to 7%. The structural and surface morphology characteristics of $Zn_{1-x}Sn_xO$ NRs/ITO composite photocatalytic films were investigated by X-Ray diffraction (XRD) and scanning electron microscopy (SEM), respectively. In addition, photocatalytic properties of synthesized materials were evaluated by degradation rates of Rhodamine-B aqueous solutions under UV light irradiation. The SEM results indicated that, with an increasing concentration of Sn dopant in $Zn_{1-x}Sn_xO$ NRs/ITO, the effective surface areas were declined by an exponential decay function and the reduction was negligible as the Sn doping concentration was higher than 3%. With the similarity in effective surface area, the contribution of Sn in the enhancement of the photocatalytic activity of $Zn_{0.93}Sn_{0.07}O$ NRs/ITO is clearly observed with 41% improvement in comparison to ZnO NRs/ITO.

1. Introduction

Recently, water pollution has become an increasingly serious issue because of rapid industrialization, increased urbanization, and overpopulation. Finding methods to clean water sources with low costs and high effectiveness is one of the most important missions of current studies. Compared to well-known traditional methods such as electrolysis and microbial decomposition, etcetera [1–4], a photocatalytic method to decompose contaminants has proved to be an outstanding method and attracted much attention of scientists around the world [5–10].

In various photocatalytic materials, ZnO has captured special attention because it is an n-type semiconductor material with stable structure, high exciton binding energy (60 meV) and, especially, a non-toxic property [11–13]. Furthermore, ZnO can be easily formed under one-dimension nanostructures [14–17] and greatly abundant in nature with low costs. However, the photocatalytic efficiency of pure ZnO materials is still quite low [18, 19]. The reason is relative to its direct wide band-gap energy. Electron and hole pairs produced during photon absorption will be rapidly recombined due to the direct band-gap energy, while wide band-gap energy allows ZnO to absorb only UV light that is about 5% of solar energy. To improve the photocatalytic activity of ZnO, metal oxides [20, 21] and noble metals such as Ag [22–24], Au [24, 25], and Pt [24, 26], were incorporated to reduce the recombination rate and collect photogenerated carriers. Besides, an ITO layer was also used as a photogenerated electron collecting layer [27]. The formed heterojunction between ITO and ZnO can separate the photogenerated electrons and holes resulting in the recombination suppression of electron-hole pairs. Using this structure, the photocatalytic rate can be enhanced up to 9.65 times faster than that of pure ZnO nanowire without an ITO layer. Furthermore, the photocatalytic ability of ZnO materials was improved by doping metals which can control the active surface area, generate lattice defects, modify bandgap energy, and

extend absorption range to visible light [28–30]. Many metals such as Al [31], Fe [32], Sn [33], Ag [34] etcetera doped in ZnO photocatalysts, are successfully utilized for the photodegradation of organic pollutants. Among these additive metals, tin (Sn) coincides with the cage structure of ZnO crystallization due to the similarity of ionic radius of Sn^{4+} and Zn^{2+} which are 0.071 nm and 0.074 nm, respectively [35]. The doping of Sn in ZnO materials is expected to change the absorption, photocatalytic and physical properties of ZnO materials. Therefore, tin is considered to be one of the most important doping elements to improve the photocatalytic activity of ZnO. However, the influences of doping concentrations of Sn and the ITO layer on the photocatalytic activity of ZnO materials, are separately investigated. Therefore, the combination of Sn dopant with various concentrations and ITO layer should be further investigated to find out its improvement in photocatalysis.

In this report, $Zn_{1-x}Sn_xO$ NRs/ITO composite photocatalytic films were studied and fabricated by a simple hydrothermal method. The Sn doping concentrations were varied from 0% to 7%. The results demonstrate that the combination between Sn dopant and ITO layer can enhance the photocatalytic activity of the $Zn_{1-x}Sn_xO$ NRs/ITO composite photocatalytic film up to 41%.

2. Experimental details

2.1. Materials

$Zn(CH_3COO)_2.2H_2O$, $Zn(NO_3)_2.6H_2O$, $C_6H_{12}N_4$, $SnCl_4$ were all purchased from Sigma. All chemicals are of analytic reagent grade and used as received without purification. ITO-coated glass was used as the substrates to support $Zn_{1-x}Sn_xO$ NRs.

2.2. Fabrication of $Zn_{1-x}Sn_xO$ NRs/ITO composite photocatalytic films

ITO-coated glass substrates with dimensions 30 mm × 30 mm were soaked in a solution containing 1.5 M NaOH for 15 min. They were then ultrasonicated in a mixture solution of acetone, ethanol, and deionized water to remove possible attached contaminants. Finally, all the substrates were completely dried and put in a clean box.

The ZnO seed layer for the subsequent step of nanorod growth was prepared as follows: Firstly, 0.1 M $Zn(CH_3COO)_2$ clear solution was prepared. 20 ml isopropyl alcohol solvent and 0.438 g $Zn(CH_3COO)_2.2H_2O$ was constantly stirred for 1 h at room temperature, then 0.5 ml diethylamine (DEA) was added drop by drop until the solution became clear and continued stirring for another hour. At the end of the process, a 0.1 M $Zn(CH_3COO)_2$ transparent solution was obtained. Secondly, the ZnO seed layer was prepared on the ITO layer by spin coating of a prepared 0.1 M $Zn(CH_3COO)_2$ transparent solution with a spin rate of 3000 rpm for 30 s. Finally, the samples were dried in the air at 150 °C for 15 min to evaporate solvents and annealed at a temperature of 450°C for 1 h.

ZnO nanorod thin films (ZnO NRs/ITO) were fabricated by a hydrothermal method by the following experimental process. The ZnO seed/ITO layers were put in an autoclave containing a 100 ml solution of 20 mM $Zn(NO_3)_2.6H_2O$, 5 mM $C_6H_{12}N_4$ (hydrothermal solution) and underwent the hydrothermal process at 80 °C for 2 h. Finally, the autoclave was slowly cooled down to room temperature, and then the samples were washed by DI water.

$Zn_{1-x}Sn_xO$ NRs/ITO composite photocatalytic films have been synthesized by the hydrothermal method by the following steps. The hydrothermal solution containing 100 ml solution of 20 mM $Zn(NO_3)_2.6H_2O$, 5 mM $C_6H_{12}N_4$ and $SnCl_4$ with various molar concentrations of Sn^{4+} (1%, 3%, 5%, and 7% in comparison with molar concentration of Zn^{2+}) were prepared in an autoclave. The ZnO seed/ITO layers were then placed in the autoclave and underwent the hydrothermal processes at 80 °C for 2 h. The autoclave was then slowly cooled down to room temperature, and then the samples were washed by DI water.

After the hydrothermal process, all the samples were subsequently annealed at 450 °C for 1 h in the air ambient.

2.3. Characterization

The surface morphologies were characterized using a field emission scanning electron microscopy (FESEM, Hitachi, S-4800). The crystal phases of the fabricated samples were determined using an X-ray diffractometer (XRD) D5000 with CuK_α radiation ($\lambda = 1.5406$ Å) over the 2θ range $20 \sim 70°$ at room temperature. The UV–Vis transmittance and absorption spectra were carried out by a UV–vis spectrophotometer (Jasco, V-670).

2.4. Photocatalytic activity measurement

The photocatalytic activity of $Zn_{1-x}Sn_xO$ NRs/ITO films were investigated by the degradation of Rhodamine B (RhB) under ultraviolet (UV) light irradiation. A sample (the surface area is 30 mm × 30 mm) was placed in 100 ml RhB solution with an initial concentration of 10 $mg.L^{-1}$. A 250 W mercury lamp was used as a UV light

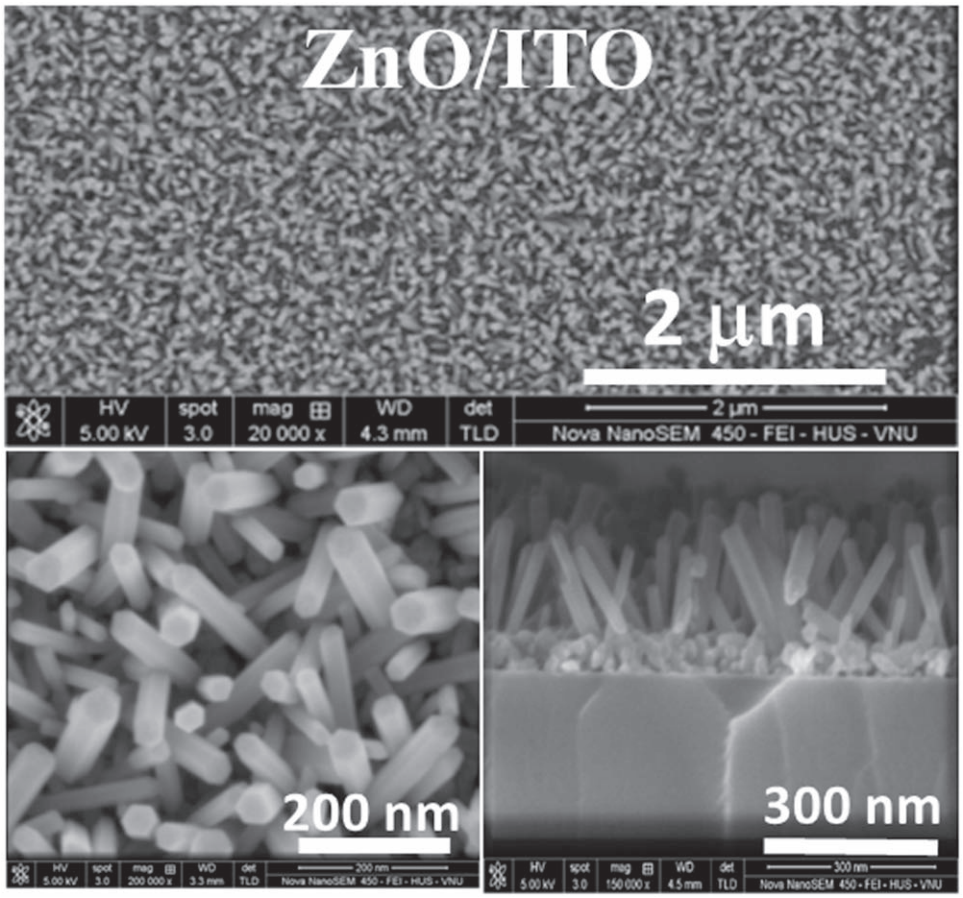

Figure 1. Top- and side-view SEM images of the ZnO NRs/ITO composite photocatalytic film.

source. After each given time interval (10 min), 2 ml solution was withdrawn and analyzed by a UV–vis spectrophotometer (Jasco, V-670) at a wavelength of 554 nm.

3. Results and discussion

Figure 1 shows the top- and side-view SEM images of the ZnO NRs/ITO composite film. This result indicates that the ZnO NRs are well-aligned and uniformly distributed. The average length, diameter, and density of the ZnO NRs are approximately of 280 nm, 35 nm, and 1.52 $\times$ 10^{10} rods/cm^2, respectively. The synthesized ZnO NRs are in a hexagonal structure.

Figure 2 illustrates the top-view SEM images of $Zn_{1-x}Sn_xO$ NRs/ITO composite photocatalytic films with variations of Sn doping concentrations from 1% to 7% (x is from 0.00 to 0.07). Even $Zn_{1-x}Sn_xO$ NRs are all in a hexagonal structure, the morphologies of the samples strongly depend on the Sn doping concentrations. This dependence is clearly indicated in figure 3 where the density of nanorods was reduced with an increase of the Sn doping concentration. The reduction of nanorod density follows an exponential decay function and the reduction was negligibly observed when the Sn doping concentration is greater than 3%. That means the nanorod densities of $Zn_{1-x}Sn_xO$ NRs/ITO as x of 0.03, 0.05, and 0.07 are relatively similar and much lower than that of ZnO NRs/ITO and $Zn_{0.99}Sn_{0.01}O$ NRs/ITO. Furthermore, as can be seen in figure 2, the diameter of the nanorods rises with an increment of Sn concentrations [36]. This is due to the different growth rates and surface energies on various crystal facets of ZnO in the nanorods' growth mechanism [37]. When the concentration of doping Sn increased, the lower nanorods' density and the higher diameter are obtained, which, subsequently, contribute to the decline of effective surface areas of $Zn_{1-x}Sn_xO$ NRs/ITO. In addition, the direction which is oriented perpendicularly to the substrate's surface is decreased when the doping concentration of Sn increases. It is due to the formation of ZnO NRs following by its *c*-axis orientation growth [38], but the appearance of dopant Sn in the crystal structure would disturb this orientation.

To investigate the crystal structure of samples, XRD studies were carried out and the results are shown in figure 4. The XRD patterns indicated that the structures of $Zn_{1-x}Sn_xO$ NRs/ITO composite films are polycrystalline. The presence of the (100), (002), (101), (102), (110), 103, and (112) peaks in the XRD patterns

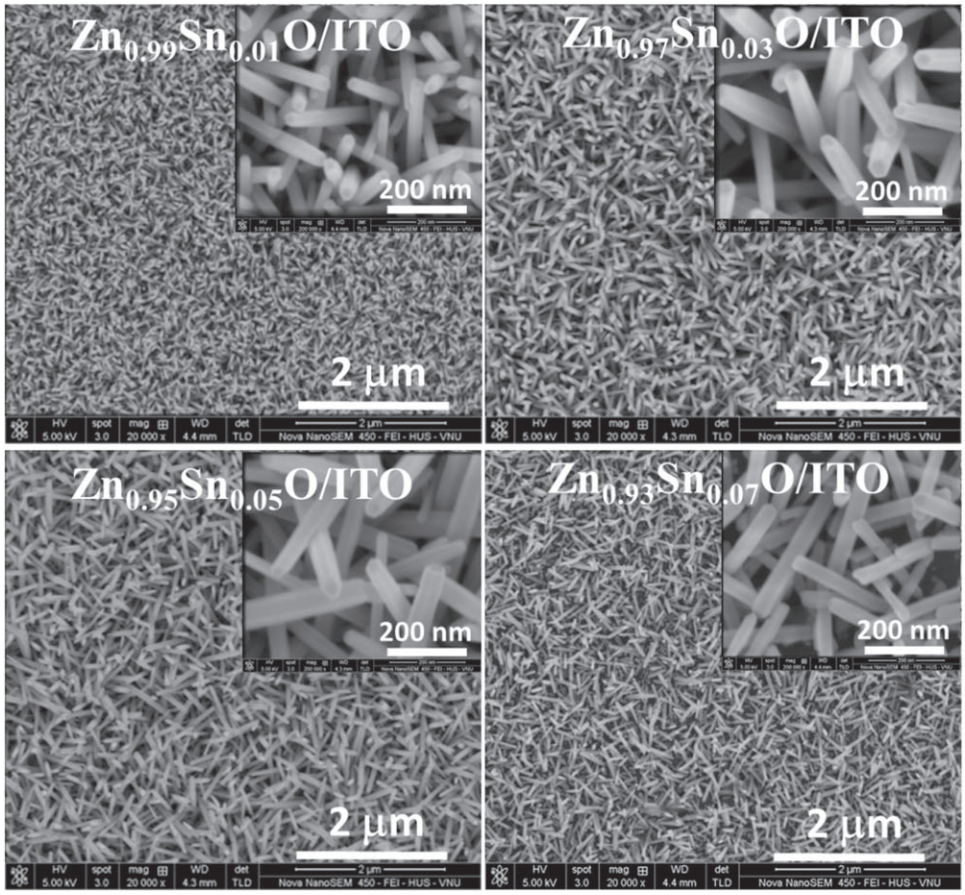

Figure 2. Top-view SEM images of $Zn_{1-x}Sn_xO$ (x = 0.01–0.07) NRs/ITO composite photocatalytic film.

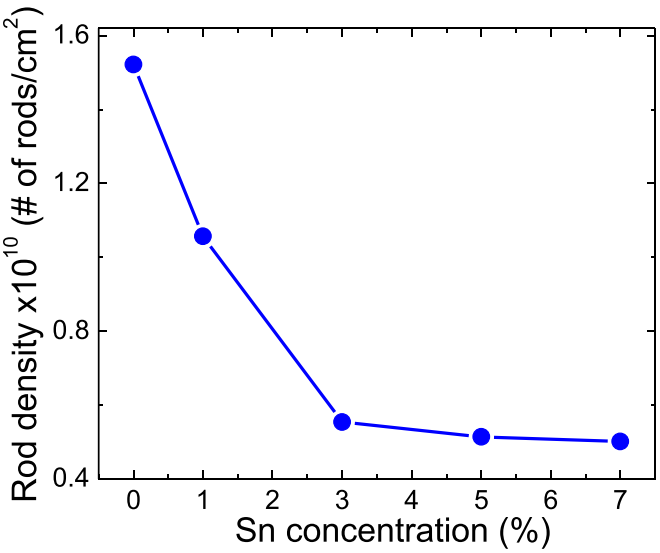

Figure 3. The dependence of rod density on the concentration of Sn dopant.

proved that $Zn_{1-x}Sn_xO$ NRs have a hexagonal wurtzite structure. The comparison of the peak intensity of the (002) peak in XRD patterns indicates that the preferential orientation along the *c*-axis direction of $Zn_{1-x}Sn_xO$ NRs/ITO composite photocatalytic films is considerably reduced if the Sn doping concentration increases. This is entirely consistent with the results obtained from SEM results. No diffraction peaks corresponding to compounds of Sn were found in the XRD patterns. That means Sn^{4+} successfully replaced Zn^{2+} in the ZnO crystal structure.

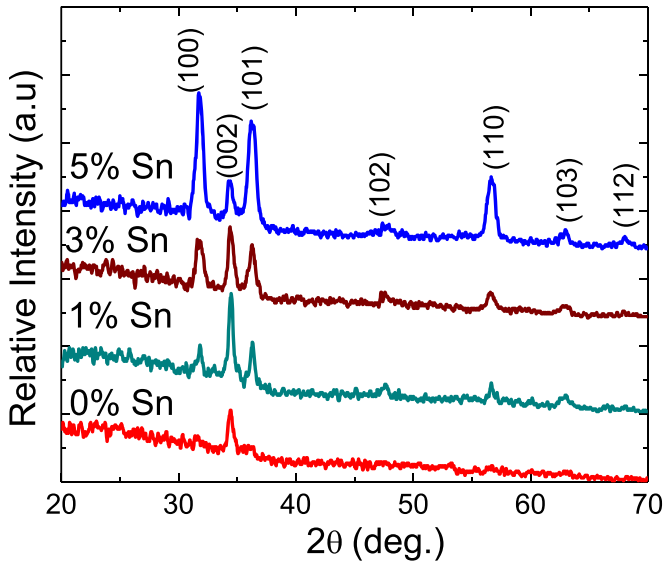

Figure 4. XRD patterns of $Zn_{1-x}Sn_xO$ NRs/ITO composite photocatalytic films.

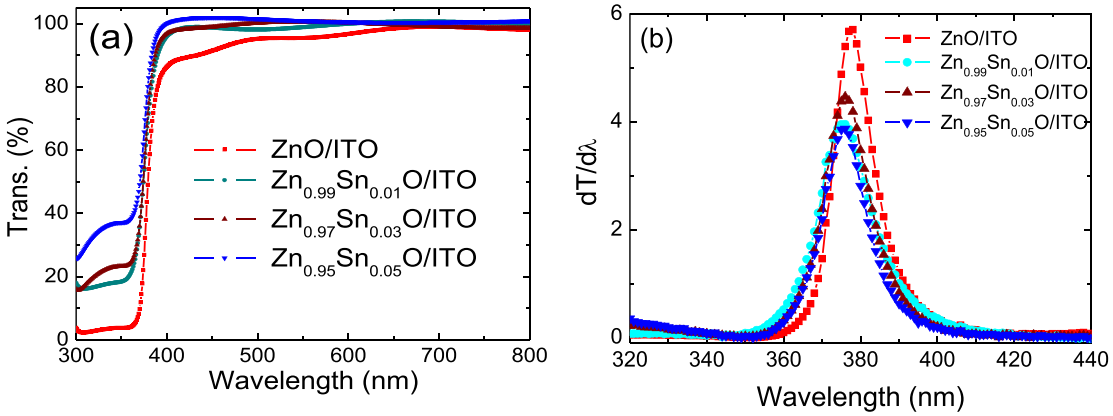

Figure 5. (a) Optical transmittance spectra of $Zn_{1-x}Sn_xO$ NRs/ITO composite photocatalytic films and (b) First derivative ($dT/d\lambda$) plot of the optical transmittance spectra of $Zn_{1-x}Sn_xO$ NRs/ITO composite photocatalytic films.

Figure 5(a) shows the transmittance spectra of $Zn_{1-x}Sn_xO$ NRs/ITO composite photocatalytic films with different Sn doping concentrations. The results indicate that the transparency of $Zn_{1-x}Sn_xO$ NRs/ITO composite photocatalytic films rise from 88.9 to 99.8% as the increment of Sn doping concentrations rise from 0 to 5%. This transmittance increment can be explained by the surface morphology of samples in figure 2. The higher Sn doping concentrations, the sparser the nanorod density was obtained which contributes to an increment of optical transmission.

The bandgap (Eg) values of $Zn_{1-x}Sn_xO$ NRs/ITO composite photocatalytic films were estimated by plotting the graph of the first derivative of transmittance ($dT/d\lambda$) versus the wavelength as shown in figure 5(b). The bandgap energies that correspond to the peaks for all of the $Zn_{1-x}Sn_xO$ NRs/ITO composite photocatalytic films were extracted as 3.289, 3.307, 3.298, 3.316, 3.324 eV when x is 0, 1, 3, 5, 7, respectively. The results indicate that the bandgap energy is slightly enlarged with the increasing Sn concentrations doped in ZnO/ITO composite photocatalytic films. This enlargement might be attributed to the enrichment of carriers in doping concentration. When the Zn^{2+} ions are replaced by Sn^{4+} ions, the carrier number is increased, which might shift the Fermi level which causes an expansion of bandgap [35].

The photocatalytic activity of $Zn_{1-x}Sn_xO$ NRs/ITO composite photocatalytic films was evaluated by the decomposition of RhB dye under the irradiation of UV light source. During the photodegradation process, the decrement of RhB concentrations was determined by a UV–vis spectrometer and shown in figure 6. The C_o and C in figure 6 are the initial concentration of RhB and the concentration of RhB at a certain reaction time, respectively. The concentration of RhB declines when reaction time increases under the illumination of UV

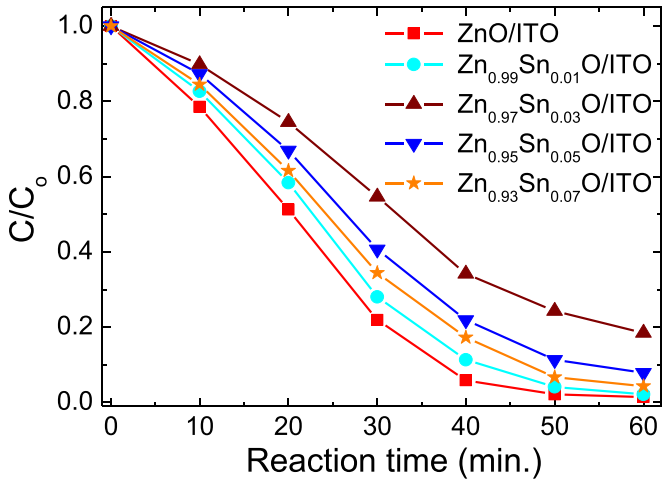

Figure 6. The photodegradation of RhB by $Zn_{1-x}Sn_xO$ NRs/ITO composite photocatalytic films.

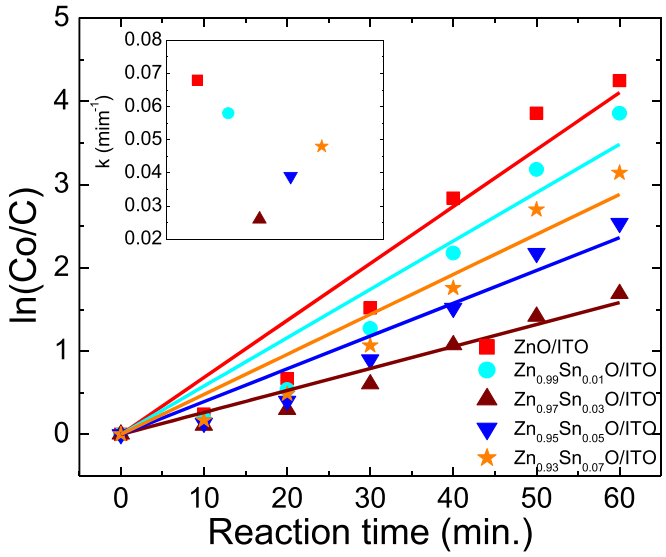

Figure 7. The first-order kinetic plot for RhB photodegradation by $Zn_{1-x}Sn_xO$ NRs/ITO composite photocatalytic films.

light. After 60 min of illumination, the degradation percentage of RhB under the catalysis of $Zn_{1-x}Sn_xO$ /ITO composite films with x of 0, 0.01, 0.03, 0.05, and 0.07 are 98, 97, 81, 92 and 95%, respectively. Furthermore, the first-order kinetics of RhB photodegradation were also calculated and replotted in figure 7. From the slopes of first-order kinetic, the pseudo-order photodegradation rate constants (k) were determined and shown in figure 7 (inset). The results indicate that the photocatalytic activity of $Zn_{1-x}Sn_xO$ NRs/ITO composite photocatalytic films is lower than that of ZnO NRs/ITO composite photocatalytic films. The photocatalytic activity of $Zn_{1-x}Sn_xO$ NRs/ITO composite photocatalytic films is contributed to by two main factors in comparison to ZnO NRs/ITO. The first one is the effectiveness of the combination between Sn dopant and ITO, and the second one is the effective surface area of nanorods. In this case, the reduction of photocatalysis of $Zn_{1-x}Sn_xO$ NRs/ITO composite photocatalytic films is heavily contributed to by the second factor which related to lower nanorod density and the larger in nanorod diameter of the Sn doped composite films (shown in figure 2). Hence, if the second factor was controlled, the enhancement effect of Sn dopant and ITO substrate on photocatalysis can be clearly observed. In details, when the $Zn_{1-x}Sn_xO$ NRs/ITO composite photocatalytic films with a doping concentration from 3% to 7% have a similarity in effective surface areas (shown in figure 2), which means the second factor was controlled nearly unchanged, the increment of degradation of RhB was observed from 81% to 95%, which is contributed to by the first factor. These results indicate that the photocatalytic activity of $Zn_{1-x}Sn_xO$ NRs/ITO composite photocatalytic films can be more efficient when the effective surface area is controlled similarity.

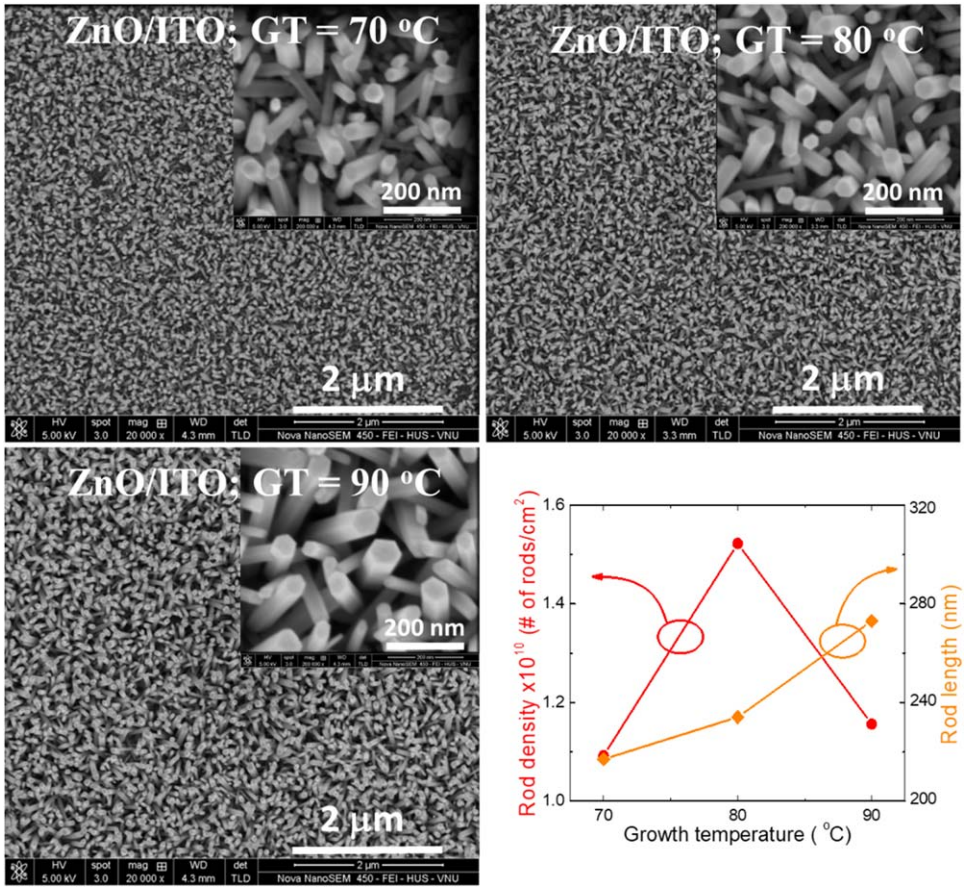

Figure 8. Top-view SEM images of the ZnO NRs/ITO composite film with variation in the effective surface areas.

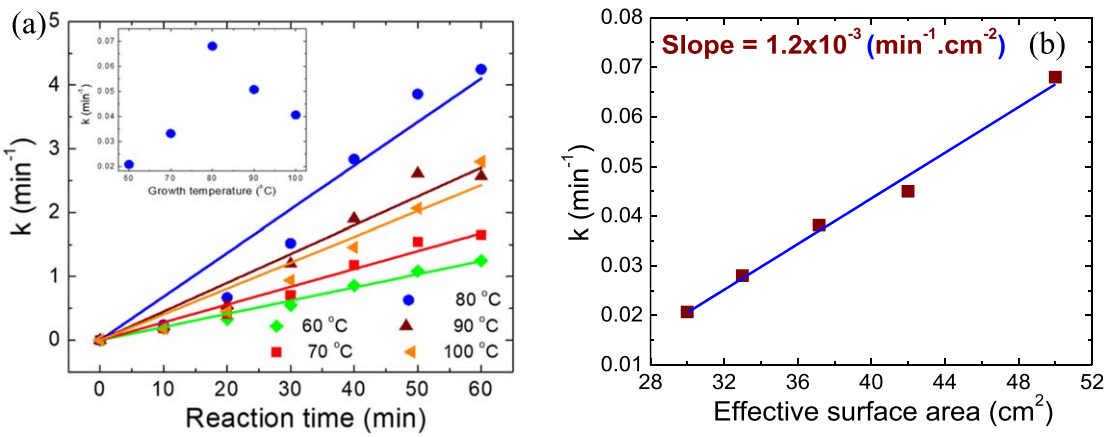

Figure 9. (a) The first-order kinetic plot for RhB photodegradation by the ZnO NRs/ITO composite photocatalytic films. (b) The pseudo-order photodegradation rate constants versus the effective surface areas.

To further evaluate the role of Sn dopant (the first factor) on photocatalysis of $Zn_{1-x}Sn_xO$ NRs/ITO composite photocatalytic films, the relationship between photodegradation rate constant (k) and effective surface areas (A) was studied by the following investigations. Firstly, the ZnO NRs/ITO composite photocatalytic films were fabricated with variation in growth temperatures from 60 to 100 °C and SEM images are shown in figure 8. These samples have different effective surface areas which vary from 30.04 cm^2 to 49.8 cm^2. Secondly, the pseudo-order photodegradation rate constant in the reaction of decomposition of RhB under UV light was investigated and depicted in figure 9(a). Finally, the relationship between photodegradation of rate constant and effective surface areas was determined from the slope of the plot of the photodegradation

rate constant versus the effective surface areas and the result is 1.2 × 10^{-3} $min^{-1}.cm^{-2}$ (figure 9(b)). Based on this result, the calculated photodegradation rate constant of ZnO NRs/ITO composite photocatalytic film is 3.4 × 10^{-2} min^{-1} corresponding to its effective surface areas of 28.3 cm^2 which is the effective surface area of the $Zn_{0.93}Sn_{0.07}O$ NRs/ITO composite photocatalytic film calculated from SEM results in figure 2. The results in figure 7 (inset) indicate that the experimental photodegradation rate constant of the $Zn_{0.93}Sn_{0.07}O$ NRs/ITO composite photocatalytic film is 4.8 × 10^{-2} min^{-1}. Therefore, the photodegradation rate constant of the $Zn_{0.93}Sn_{0.07}O$ NRs/ITO composite photocatalytic film can be improved up to 41% compared to that of the ZnO NRs/ITO composite photocatalytic film. This improvement is contributed to by the role of Sn dopant in composite films.

4. Conclusions

$Zn_{1-x}Sn_xO$ NRs/ITO composite photocatalytic films were successfully fabricated by the hydrothermal method. The Sn doping concentrations have a strong influence on the effective surface areas of $Zn_{1-x}Sn_xO$ NRs/ITO composite photocatalytic films. The reduction of effective surface areas followed an exponential decay function and the negligible reduction was observed when Sn doping concentration is higher than 3%. With the similarity in effective surface area, the photodegradation rate constant of the $Zn_{0.93}Sn_{0.07}O$ NRs/ITO composite photocatalytic film can be improved up to 41% compared to that of the ZnO NRs/ITO composite photocatalytic film. Therefore, the Sn dopant was proved to contribute to the enhancement of the photocatalytic activity of $Zn_{1-x}Sn_xO$ NRs/ITO composite photocatalytic films.

Acknowledgments

This research was supported by the Vietnam National Foundation for Science and Technology Development (NAFOSTED) under Grant Number 103.99-2019.19.

ORCID iDs

Dinh Lam Nguyen https://orcid.org/0000-0002-4349-6830

References

[1] Shah Walter S R, Jaekel U, Osterholz H, Fisher A T, Huber J A, Pearson A and Girguis P R 2018 Microbial decomposition of marine dissolved organic matter in cool oceanic crust *Nat. Geosci.* **11** 334–9
[2] Boopathy R, Beary T and Templet P J 2001 Microbial decomposition of post-harvest sugarcane residue *Bioresour. Technol.* **79** 29–33
[3] Chen Z, Gong X, Wang Z, Wang Y, Zhang S and XU D 2013 Sulfur removal from ionic liquid-assisted coal water slurry electrolysis in KNO3 system *Journal of Fuel Chemistry and Technology* **41** 928–36
[4] Aghahosseini S, Dincer I and Naterer G F 2013 Linear sweep voltammetry measurements and factorial design model of hydrogen production by HCl/CuCl electrolysis *Int. J. Hydrogen Energy* **38** 12704–17
[5] Ratnayake S P, Mantilaka M M M G P G, Sandaruwan C, Dahanayake D, Murugan E, Kumar S, Amaratunga G A J and Nalin D S K M 2018 Carbon quantum dots-decorated nano-zirconia: a highly efficient photocatalyst *Appl. Catal., A* **570** 23–30
[6] Hua S, Qu D, An L, Jiang W, Wen Y, Wang X and Sun Z 2018 Highly efficient p-type Cu3P/n-type g-C3N4 photocatalyst through Z-scheme charge transfer route *Appl. Catalysis B* **240** 253–61
[7] Yu C L, Liu H, Song J, Yang J, Zhang P C, Guo F L, Hong L and Hui H B 2019 Can mixed anatase and rutile photocatalyst TiO_2 be synthesized under high pressure in water? *Mater. Lett.* **246** 133–6
[8] Kato K, Vaucher S, Hoffmann P, Xin Y and Shirai T 2018 A novel single-mode microwave assisted synthesis of metal oxide as visible-light photocatalyst *Mater. Lett.* **235** 125–8
[9] Chauhan M, Soni K, Karthik E K, Reddy K P, Chinnakonda G S and Deka S 2019 A promising visible-light driven hydrogen production from water on highly efficient $CuCo_2S_4$ nanosheets photocatalyst *Journal of Materials Chemistry A* 6985–94
[10] Duan Z, Huang Y, Zhang D and Chen S 2019 Electrospinning fabricating Au/TiO_2 network-like nanofibers as visible light activated photocatalyst *Sci. Rep.* **9** 8008
[11] Wang S, Zhu B, Liu M, Zhang L, Yu J and Zhou M 2018 Direct Z-scheme ZnO/CdS hierarchical photocatalyst for enhanced photocatalytic H_2-production activity *Appl. Catalysis B* **243** 19–26
[12] Ding W *et al* 2019 Bovine serum albumin assisted synthesis of Ag/Ag_2O/ZnO photocatalyst with enhanced photocatalytic activity under visible light *Colloids Surf., A* **568** 131–40
[13] Seong S *et al* 2019 Synthesis of Ag-ZnO coreshell nanoparticles with enhanced photocatalytic activity through atomic layer deposition *Mater. Des.* **177** 107831
[14] Braiek Z, Roques-Carmes T, IBen A, Gannouni M, Arnoux P, Corbel S and Chtourou R 2018 Enhanced solar and visible light photocatalytic activity of In2S3-decorated ZnO nanowires for water purification *Journal of Photochemistry and amp; Photobiology, A: Chemistry* **368** 307–16
[15] Jiang Y, Liao J-F, Xu Y-F, Chen H-Y, Wang X-D and Kuang D-B 2019 Hierarchical $CsPbBr_3$ nanocrystal decorated ZnO nanowires/macroporous graphene hybrids for enhancing charge separation and photocatalytic CO_2 reduction *Journal of Materials Chemistry A.* 13762–9

[16] Smazna D, Shree S, Polonskyi O, Lamaka S, Baum M, Zheludkevich M, Faupel F, Adelung R and Mishra Y K 2019 Mutual interplay of ZnO micro- and nanowires and methylene blue during cyclic photocatalysis process *Journal of Environmental Chemical Engineering* **7** 103016
[17] Singh R and Dutta S 2019 The role of pH and nitrate concentration in the wet chemical growth of nano-rods shaped ZnO photocatalyst *Nano-Structures & Nano-Objects* **18** 100250
[18] Ahmad M, Ahmed E, Zhang Y, Khalid N R, Xu J, Ullah M and Hong Z 2013 Preparation of highly efficient Al-doped ZnO photocatalyst by combustion synthesis *Curr. Appl Phys.* **13** 697–704
[19] Anandan S, Ohashi N and Miyauchi M 2010 ZnO-based visible-light photocatalyst: Band-gap engineering and multi-electron reduction by co-catalyst *Appl. Catalysis B* **100** 502–9
[20] Tawfik W Z, Hassan M A, Johar M A, Ryu S-W and Lee J K 2019 Highly conversion efficiency of solar water splitting over p-Cu_2O/ZnO photocatalyst grown on a metallic substrate *J. Catal.* **374** 276–83
[21] Sánchez-Cid P, Jaramillo-Páez C, Navío J A, Martín-Gómez A N and Hidalgo M C 2019 Coupling of Ag_2CO_3 to an optimized ZnO photocatalyst: advantages vs. disadvantages *J. Photochem. Photobiol., A* **369** 119–32
[22] Vignesh S *et al* 2019 Highly efficient visible-light photocatalytic and antibacterial performance of PVP capped Cd:Ag: ZnO photocatalyst nanocomposites *Appl. Surf. Sci.* **479** 914–29
[23] Zare M *et al* 2019 Novel green biomimetic approach for synthesis of Zno-Ag nanocomposite; antimicrobial activity against food-borne pathogen, biocompatibility and solar photocatalysis *Sci. Rep.* **9** 8303
[24] Vaiano V, Jaramillo-Paez C A, Matarangolo M, Navío J A and del Carmen Hidalgo M 2019 UV, and visible-light driven photocatalytic removal of caffeine using ZnO modified with different noble metals (Pt, Ag, and Au) *Mater. Res. Bull.* **112** 251–60
[25] Ye Y, Wang K, Huang X, Lei R, Zhao Y and Liu P 2019 Integrating piezoelectric effect into Au/ZnO photocatalyst for efficient charges separation *Catalysis Science & Technology* **9** 3771–8
[26] Zayed M, Ahmed A M and Shaban M 2019 Synthesis and characterization of nanoporous ZnO and Pt/ZnO thin films for dye degradation and water splitting applications *Int. J. Hydrogen Energy* **44** 17630–48
[27] Cui R, Shen K, Xu M, Xiang D and Xu Q 2016 Enhancing photocatalytic activity of ZnO nanowires by embedding ITO layer as a photogenerated electron collecting layer *Mater. Sci. Semicond. Process.* **43** 155–62
[28] Singh D P 2010 Synthesis and growth of ZnO nanowires *Science of Advanced Materials* **2** 245–72
[29] Yi G S, Lu H C, Zhao S Y, Yue G, Yang W J, Chen D P and Guo L H 2004 Synthesis, characterization, and biological application of size-controlled nanocrystalline $NaYF_4$:Yb, Er infrared-to-visible up-conversion phosphors *Nano Lett.* **42** 2191–6
[30] Wang L, Yan R X, Hao Z Y, Wang L, Zeng J H, Bao J, Wang X, Peng Q and Li Y D 2005 Fluorescence resonant energy transfer biosensor based on upconversion-luminescent nanoparticles *Angew. Chem. Int. Ed.* **44** 6054–7
[31] Baradaran M, Ghodsi F E, Bittencourt C and Llobet E 2019 The role of Al concentration on improving the photocatalytic performance of nanostructured ZnO/ZnO:Al/ZnO multilayer thin films *J. Alloys Compd.* **788** 289–301
[32] Han C, Duan L, Zhao X, Hu Z, Niu Y and Geng W 2018 Effect of Fe doping on structural and optical properties of ZnO films and nanorods *J. Alloys Compd.* **770** 854–63
[33] Xu L, Zheng G, Xian F and Su J 2019 The morphological evolution of ZnO thin films by Sn ions doping and its influence on the surface energy and photocatalytic activity *Mater. Chem. Phys.* **229** 215–25
[34] Li X, He S, Liu X, Jin J and Meng H 2018 Polymer-assisted freeze-drying synthesis of Ag-doped ZnO nanoparticles with enhanced photocatalytic activity *Ceram. Int.* **45** 494–502
[35] Dhamodharan P, Manoharan C, Dhanapandian S, Bououdina M and Ramalingam S 2015 Preparation and characterization of spray deposited Sn-doped ZnO thin films onto ITO subtracts as photoanode in dye sensitized solar cell *Journal of Material Science: Materials in Electrons* **2** 10–28
[36] Wu C, Shen L, Yu H, Huang Q and Zhang Y C 2011 Synthesis of Sn-doped ZnO nanorods and their photocatalytic properties *Mater. Res. Bull.* **46** 1107–12
[37] Gu Y S, Qi J J and Zhang Y 2007 Surface energy of in-doped ZnO STUDIED by PAW + U method *Mater. Sci. Forum* **561–565** 1861–4
[38] Shi Z-F, Zhang Y-T, Cai X-P, Wang H, Wu B, Zhang J-X and Du G-T 2014 Parametric study on the controllable growth of ZnO nanostructures with tunable dimensions using catalyst-free dye-sensitized chemical vapor deposition *Cryst. Eng. Comm.* **16** 455–63